Experimental Neurology 383 (2025) 115000

Contents lists available at ScienceDirect

Experimental Neurology

journal homepage: www.elsevier.com/locate/yexnr

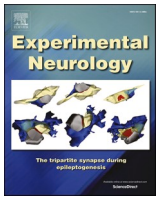

Research paper

METTL5-mediated 18S rRNA m^{6}A modification promotes corticospinal tract sprouting after unilateral traumatic brain injury

Zhenpeng Li [a,b,1], An Jiang [a,b,1], Jintao Fang [a,b,1], Yifei Jiang [a,b,1], Wenting He [a,b], Liwei Yan [a,b], Shuai Qiu [c], Bengang Qin [a,b], Qingtang Zhu [a,b], Honggang Wang [a,b,*]

[a] Department of Microsurgery, Orthopedic Trauma and Hand Surgery, The First Affiliated Hospital, Sun Yat-sen University, Guangzhou 510080, China
[b] Guangdong Provincial Key Laboratory of Orthopedics and Traumatology, Guangzhou 510080, China
[c] Department of Orthopedics, The Eighth Affiliated Hospital, Sun Yat-sen University, Shenzhen 518033, China

ARTICLE INFO

Keywords:
Unilateral brain injury
Corticospinal tract sprouting
Axon outgrowth
METTL5
18S rRNA
m^{6}A modification
Translation efficiency
Cofilin

ABSTRACT

The key to improving function of an impaired limb after unilateral brain injury is promotion of corticospinal tract (CST) sprouting across the midline into the denervated hemicord. Previous studies have unveiled specific genes that regulate CST sprouting. CST sprouting may also be regulated by RNA modification. We examined METTL5, the methyltransferase for 18S rRNA m^{6}A modification, as a regulator of CST sprouting in mice. Overexpression of METTL5 in contralesional corticospinal neurons promoted CST sprouting after unilateral traumatic brain injury. Mechanically, METTL5-mediated 18S rRNA m^{6}A modification promoted the translation efficiency (TE) of various genes. Notably, the upregulation of TE in the gene *Cfl1,* which encodes cofilin, led to an increase in its expression. Additionally, the upregulation of TE in the gene *Inpp5k* led to the activation of cofilin. Active cofilin stimulates actin polymerization and facilitates protrusion and bundling of microtubules, thus promoting axon outgrowth. These findings offer valuable insights for developing novel strategies to promote CST sprouting.

1. Introduction

Unilateral brain injury caused by ischemia, trauma, or infection results in asymmetric neurological deficits and asymmetry in posture and balance (Bakalkin et al., 2021). Spontaneous recovery from small lesions (<10 %–15 % of the cortex) is frequently good owing to compensation of the adjacent cortex (Liepert et al., 2000; Starkey et al., 2012). Large lesions (> 40 %) typically result in permanent neurological dysfunction (Biernaskie et al., 2005). Larger lesions are associated with corticospinal tract (CST) sprouting, a process in which axons from contralateral corticospinal neurons (CSNs) generate collateral branches that sprout across the midline into the denervated spinal hemicord (Lindau et al., 2014). CST sprouting establishes a connection between the contralesional motor cortex and denervated spinal motoneurons, making it instrumental in enhancing neurological recovery (Liu et al., 2021; Boato et al., 2023; Yang et al., 2024). However, the effect is constrained because of the limited potential of spontaneously sprouting CST axons (Murphy and Corbett, 2009; Benowitz and Carmichael, 2010). In select patients with upper limb impairment caused by unilateral brain injury, contralateral C7 nerve transfer surgery is performed in an attempt to regain function. Its effect is achieved by enhancing CST sprouting (Zheng et al., 2018; Gao et al., 2022). However, the underlying molecular mechanism remains elusive.

Recent studies have unveiled specific genes that regulate CST sprouting, such as *Eef1a*-(Romaus-Sanjurjo et al., 2022), *Ngr1* (Fink et al., *2017*), *Inpp5k*-(Kauer et al., 2022), *Pten* and *Socs3* (Jin et al., *2015*). CST sprouting may also be regulated *via* RNA modifications. Modifications of transfer RNA (tRNA) regulate tRNA stability, thereby affecting the translation efficiency (TE) of numerous genes (Duechler et al., 2016). Dysregulation of tRNA modification may result in several developmental diseases (Xia et al., 2023). Modifications of messenger RNA (mRNA) affect gene expression by their effects on mRNA splicing, export, transport, and translation (Zhao et al., 2017; Pandolfi, 2004). A recent study even found that mRNA m^{6}A modification has an important influence on axon regeneration (Wang et al., 2023).

Ribosomal RNA (rRNA) accounts for more than 80 % of all cellular

* Corresponding author.
E-mail address: whongg@mail.sysu.edu.cn (H. Wang).
[1] These authors contributed equally to this work.

https://doi.org/10.1016/j.expneurol.2024.115000
Received 15 July 2024; Received in revised form 7 October 2024; Accepted 11 October 2024
Available online 13 October 2024

RNA (Noller, 1991) and contains diverse modifications. rRNA modification is crucial for stress resistance and lifespan in yeast and worms (Schosserer et al., 2015). Its significance in neural development has been recently recognized, particularly in development of the corpus callosum and neuron migration (Chen et al., 2019; Yuan et al., 2019). The 18S rRNA m^6A methyltransferase METTL5 is particularly crucial for brain development, as mutations in its gene result in intellectual disability and microcephaly (Richard et al., 2019). However, whether METTL5 regulates CST sprouting after unilateral brain injury is not known. This study aims to investigate the role and underlying mechanisms of METTL5 in CST sprouting following unilateral traumatic brain injury (TBI).

2. Material and methods

2.1. Mice

All experiments were approved by the Ethics Committee of The First Affiliated Hospital, Sun Yat-sen University (approval number: [2023] 148). Eight-week-old male wild-type (WT) C57BL/6 mice were provided from the Laboratory Animal Center of Sun Yat-sen University. Mice were randomly assigned to different groups, treated according to the National Research Council's guidelines for the Care and Use of Laboratory Animals, and had free access to food and water (temperature 20°-26 °C, relative humidity 40 %–70 %, 12-h light/dark cycle).

2.2. Cortical AAV injection

Transduction of CSNs in the right primary motor cortex (M1 region) using adeno-associated virus (AAV) was executed using a previously described method (Gao et al., 2022; Kauer et al., 2022). Before injection, AAV9-CAG-*Mettl5*-flag (customized by PackGene, China) + AAV9-CAG-GFP (customized by PackGene) or AAV9-CAG-DIO-mCherry (customized by BrainVTA, China) + AAV9-CAG-GFP were mixed, the final concentration of each virus was 5×10^{12} viral particles/mL. Mice were anesthetized using 1 %–2 % isoflurane and then secured in a stereotaxic apparatus (RWD Life Science, China). Through the midline incision on the scalp, a burr hole was made to expose the right cortex using a cranial drill (RWD Life Science). The coordinates of the burr hole were − 1 to +1 mm posterior to the bregma and 0.5 to 1.5 mm lateral. Subsequently, 1 μL of viral solution was injected *via* a glass micropipette into five random points in the burr hole at a depth of 0.7 mm using Nanoject III (Drummond Scientific, USA). After each injection, the micropipette was kept in place for 5 to 10 min before it was slowly retracted. The scalp was sutured following the procedure.

2.3. Establishment of unilateral TBI

All mice were subjected to a unilateral TBI procedure two weeks after AAV injection. Unilateral TBI was completed as previously described (Wu et al., 2021). Following induction of anesthesia as described above, mice were positioned in a stereotaxic apparatus and a midline scalp incision was made to expose the skull. Subsequently, a 3-mm-diameter craniectomy was performed using a cranial drill to expose the left cortex. The coordinates of the craniectomy were − 1.0 to +2.0 mm anterior to the bregma and 0.5 to 3.5 mm lateral. A contusion was then induced using a precise impactor (RWD Life Science) equipped with a head hammer with a diameter of 3 mm. The impact contusion depth was set at 1.25 mm from the dura with a preset velocity of 4.0 m/s and sustained for 100 ms. These injury parameters were chosen to target the motor cortex of the left hemisphere. Absorbable hemostatic sponges were employed during the procedure to control bleeding. The scalp was sutured following the procedure.

2.4. Behavioral tests

Recovery of the impaired forelimb was evaluated using the grid walking and cylinder tests. All experimental mice underwent testing the day before TBI and days 3, 7, 14, 21, and 28 after. The data obtained on the day before was considered baseline. All outcome analyses were performed by an independent investigator who was blinded to the experimental groups.

The grid walking test evaluates the accuracy of paw placement on the rungs of an elevated grid during spontaneous exploration. Mice were placed on an elevated 25 × 25 cm metal grid with 2.5 × 2.5 cm squares and allowed to freely explore for 3 min. Their performance was recorded using a video camera. Missed steps were recorded either when the paw completely fell between rungs or when part of the paw made contact with a rung instead of proper grasping. The missed step rate for the impaired forelimb was calculated as missed steps/total steps × 100 %.

The cylinder test assesses forelimb asymmetry during spontaneous exploration. Mice were placed in a transparent cylinder (9 cm in diameter and 15 cm in height) and their spontaneous rearing was videotaped for 5 min. The duration of contact of each paw with the wall during rearing was recorded and the percentage of contact time of each limb calculated. These data were used to determine an asymmetry index (the percentage of left paw contact time minus the percentage of right paw contact time).

2.5. Histology and immunohistochemistry

Mice were euthanized immediately using CO_2 and subjected to transcardial perfusion with normal saline containing 10 U/mL heparin, followed by perfusion with 4 % paraformaldehyde (PFA) in phosphate-buffered saline (PBS). The brain and C5 and C6–7 spinal cord were then dissected, postfixed overnight in 4 % PFA in PBS, and dehydrated in a 30 % sucrose solution in PBS for 3 days. Using a cryostat (CM1950, Leica, Germany), the brain samples were sliced into 20-μm coronal sections; the spinal cord samples were sliced into 20-μm transverse sections. Sections were washed three times with PBS and blocked with Quick-Block Blocking Buffer (Beyotime, Cat# P0260, China) for 10 min. Then, sections were incubated with primary antibodies targeting GFP (mouse, 1:200, Proteintech, Cat# 66002-1-Ig, China), flag (rabbit, 1:1000, Proteintech, Cat# 80010-1-RR) or PKCγ (rabbit, 1:200, Cell Signaling Technology, Cat# 59090, USA) overnight at 4 °C, followed by secondary antibodies including Alexa Fluor 488-conjugated goat anti-mouse IgG (1:1000, Abcam, Cat# ab150113, UK) or Alexa Fluor 555-conjugated goat anti-rabbit IgG (1:1000, Abcam, Cat# ab150078) for 2 h at room temperature. Nuclei were stained with DAPI (Solarbio, Cat# C0065, China) for 15 min. Images were captured using a fluorescence microscope (DMi8, Leica) and evaluated as previously described (Kauer et al., 2022). To determine the total number of CST axons labeled, five images of the C5 spinal cord dorsal column were taken from each mouse. A 25 × 25 μm grid was then overlaid on the images and the number of GFP^+ axons in three randomly selected boxes from the grid was counted. The average number of axons from these boxes was then scaled by the total area occupied by GFP^+ axons in the dorsal column to determine the total number of labeled axons. To determine the number of sprouting CST axons, five images of the C6–7 spinal cord were taken from each mouse. The midline was drawn from the base of the dorsal columns through the ventral medial fissure and the average number of individual GFP^+ CST axons crossing the midline was counted. An independent investigator who was blinded to the experimental groups conducted the analyses.

2.6. Cerebral cortical neuron cultures and plasmid transfection

Cerebral cortical neurons were cultured using a previously described method (Zhu et al., 2023). The cerebral cortices from embryos at 17 days (E17) were rapidly extracted from WT pregnant C57BL/6 mice. After the meninges were dissected, the cortices were cut into scrapes. These tissue scrapes were then digested for 20 min at 37 °C in a digestion medium containing DMEM medium with high glucose (Thermo Fisher Scientific, Cat# C11965500BT, USA) with papain (1 mg/mL, Solarbio, Cat#

Table 1
The sequences for primers and probes in qRT-PCR and SELECT.

Name	Sequence (5′-3′)
Mettl5	Forward: TGAAAACAAAGCGGTTGCAGAT
	Reverse: TAGGAGTGGGGAGTGGACAG
Cfl1	Forward: AGACAAGGACTGCCGCTATG
	Reverse: TTGCTCTTGAGGGGTGCATT
β-Actin	Forward: GATCTGGCACCACACCTTCT
	Reverse: GGGGTGTTGAAGGTCTCAAA
18S m^6A at site 1832	up probe: TAGCCAGTACCGTAGTGCGTGGGTTCACCTACGGAAACCTTG
	down probe: phos/TACGACTTTTACTTCCTCTAGATAGTCAAGCAGAGGCTGAGTCGCTGCAT
qRT-PCR for SELECT	Forward: ATGCAGCGACTCAGCCTCTG
	Reverse: TAGCCAGTACCGTAGTGCGTG

Note: SELECT: single-base elongation and ligation-based PCR amplification.

G8430) and DNase I (1000 U/mL, Beyotime, Cat# D7076). After digestion, the mix cells were filtered through a 40-mm cell sieve and counted and then seeded in 10-cm culture dishes, 6-well or 24-well plates precoated with poly-L-lysine (Solarbio, Cat# P8130) and incubated with the basal medium composed of DMEM medium with high glucose with 10 % fetal bovine serum (Zeta Life, Cat# Z7181FBS-500, USA) and 1 % penicillin-streptomycin (Thermo Fisher Scientific, Cat# 15140122).

Four hours after seeding, either overexpression plasmids (pLVX-CAG-*Mettl5*-flag) or control plasmids (pLVX-vector) were applied to the cortical neurons for overexpressing target genes or control. PolyShooter HP Transfection Regent (LeapWal, Cat# P19110, China) was used to transfect the plasmids into cells following the manufacturer's instructions. These cells were incubated with the neuronal culture medium composed of Neurobasal (Thermo Fisher Scientific, Cat# 21103049) with 2 % B27 supplement (Thermo Fisher Scientific, Cat# 17504044), 1 % GlutaMAX (Thermo Fisher Scientific, Cat# 35050061) and 1 % penicillin-streptomycin for three days at 37 °C with 5 % CO_2.

2.7. RNA extraction, reverse transcription and qRT-PCR

Total RNA from cells in 6-well plates were extracted using Trizol reagent (Thermo Fisher Scientific, Cat# 15596026CN). HiScript III RT SuperMix for qRT-PCR Kit (Vazyme, Cat# R323-01, China) was used for reverse transcription. The cDNA samples were diluted and used for qRT-PCR using the TB Green Premix Ex Taq II Kit (Takara, Cat# RR820A, Japan) in the LightCycler 480 real-time PCR system (Roche, Switzerland). β-actin was used as an internal control. The relative mRNA expression levels of target genes were calculated using the $2^{-\Delta\Delta Ct}$ method. The results were from three separate experiments. The primers are listed in Table 1.

2.8. SELECT

The single-base elongation and ligation-based PCR amplification (SELECT) was performed using the Epi-SELECT m^6A site identification kit (EP-biotek, Cat# R202106M-01, China). In brief, the designed up and down probes flanking the m^6A at site 1832 were annealed, followed by extension of a single base using SELECT DNA polymerase and nicking of the junction using SELECT Ligase. m^6A levels in the targeted region were measured using qRT-PCR assays. The probes and primers are listed in Table 1.

2.9. RNA-seq and data analysis

RNA sequencing (RNA-seq) was performed by Shanghai Bioprofile Co., Ltd., China. In brief, total RNA from cells in 6-well plates was extracted using Trizol reagent. Then, cDNA libraries were constructed for high-throughput sequencing. The gene-expression level was normalized using fragments per kilobase of exon per million mapped fragments (FKPM). Genes that exhibited a fold change of METTL5/Control greater than 1.5 or less than 0667, coupled with a *p*-value of less than 0.05, were classified as differentially transcribed genes. Gene Ontology analysis was conducted using the Knowledge-Based Annotation System for intelligent analysis (http://bioinfo.org/kobas/).

2.10. RNC-seq and data analysis

Ribosome nascent-chain complex-bound mRNA-seq (RNC-seq) was performed as previously described (Wang et al., 2013). Cells in 10-cm culture dishes were treated with 100 μg/mL cycloheximide for 15 min and then collected and lysed in 1.2 mL lysis buffer containing 1 % Triton X-100 in ribosome buffer (RB buffer; which contains 20 mM HEPES-KOH [pH 7.4,], 15 mM $MgCl_2$, 200 mM KCl, 100 μg/mL cycloheximide, and 2 mM dithiothreitol) for 30 min on ice. Cell lysates were centrifuged at 16,200*g* for 10 min at 4 °C to remove the cell debris. Then 10 % of the supernatant was used as input control. The remaining supernatant were transferred on the surface of 12 mL of RB buffer containing 30 % sucrose. RNC-mRNAs were pelleted after ultracentrifugation at 185000*g* for 5 h at 4 °C. The input samples and RNC-mRNAs were extracted using Trizol reagent and subjected to RNA-seq by Shanghai Bioprofile Co., Ltd., China.

The gene expression level was normalized using transcripts per kilobase of exon model per million mapped reads (TPM). TE was calculated using the following formula: TE = (TPM in RNC-seq)/(TPM in input RNA-seq). Genes that exhibited a TE ratio of METTL5/Control greater than 1.5 or less than 0.667 were classified as differentially translated genes. Gene Ontology analysis was conducted using the Knowledge-Based Annotation System for intelligent analysis.

2.11. Western blot

Total protein of cells in 6-well plates was extracted using RAPA (Meilunbio, Cat# MA0151, China) with protease inhibitor (EpiZyme, Cat# GRF101, China) and phosphatase inhibitor (EpiZyme, Cat# GRF102). Protein samples were separated on a PAGE gel by electrophoresis and then transferred to polyvinylidene fluoride membranes (Millipore, USA). Blots were blocked using Protein Free Rapid Blocking Buffer (EpiZyme, Cat# PS108P) and then incubated with primary antibodies targeting METTL5 (rabbit, 1:1000, Affinity, Cat# DF13232, China), cofilin (mouse, 1:1000, Proteintech, Cat# 66057-1-Ig), p-cofilin (rabbit, 1:1000, Affinity, Cat# AF3232), INPP5K (rabbit, 1:000, Proteintech, Cat# 15098-1-AP) or β-actin (mouse, 1:20000, Proteintech, Cat# 66009-1-Ig) overnight at 4 °C, followed by horseradish peroxidase-conjugated secondary antibodies including anti-rabbit IgG (1:5000, Cell Signaling Technology, Cat# 7074) or anti-mouse IgG (1:5000, Cell Signaling Technology, Cat# 7076) for 2 h at room temperature. The ECL Chemiluminescence Kit (Tanon, Cat# 180-5001, China) was used to visualize the protein bands. ImageJ software (National Institutes of Health, USA) was applied to analyze the gray intensities of protein bands. The results were from three separate experiments.

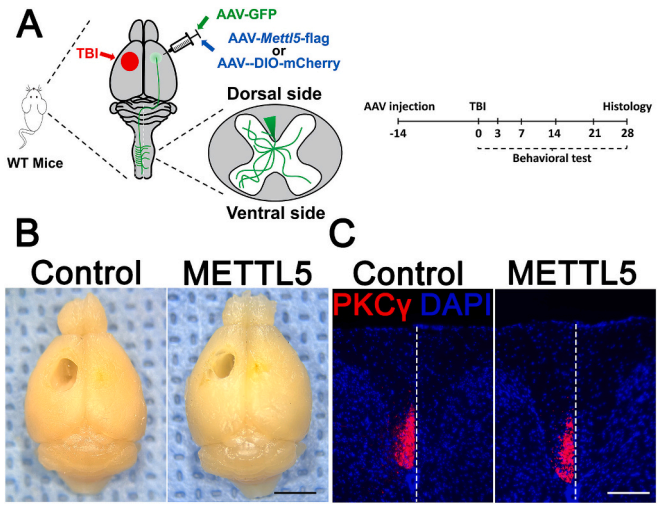

Fig. 1. Schematic and establishment of the mouse model of unilateral traumatic brain injury. (A) The schematic shows the relative locations of unilateral brain injury and injections of AAV-*Mettl5*-flag or AAV-DIO-mCherry (control) + AAV-GFP. The Inset shows GFP$^+$ corticospinal tract axons in transverse cervical section, which was subject to analysis; right, experimental timeline. (B) Images of brain morphology from mice 28 days after unilateral injury. Scale bar: 4 mm. (C) Immunofluorescent images of PCKγ in transverse sections of the C5 spinal cord from mice 28 days after unilateral injury. Scale bar: 200 μm. AAV: adeno-associated virus; TBI: traumatic brain injury; WT: wild type.

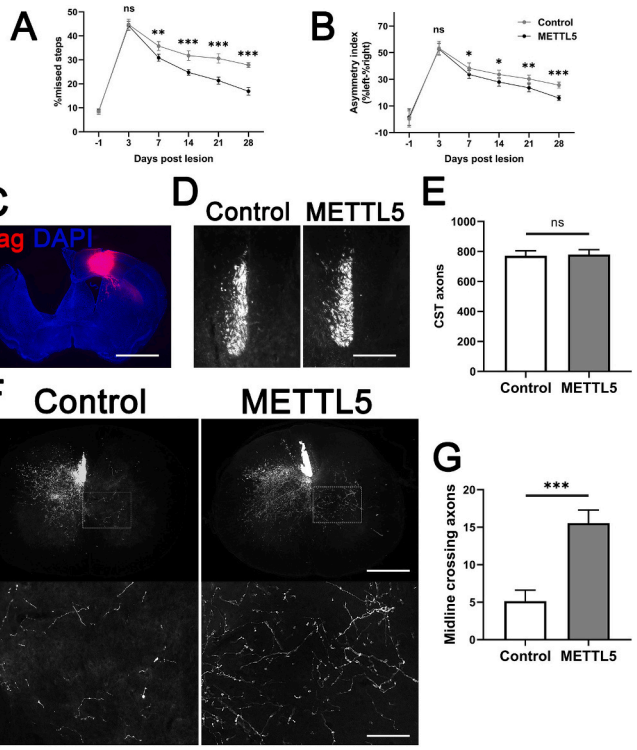

Fig. 2. METTL5 promotes corticospinal tract sprouting in mice after unilateral traumatic brain injury. (A, B) Behavioral tests, including the grid walking test (A) and the cylinder test (B), to evaluate impaired forelimb function in mice treated with AAV-DIO-mCherry or AAV-*Mettl5*-flag within the 28-day period after unilateral brain injury (n = 6 each). (C) Immunofluorescent image of flag in coronal brain section from mice 42 days after AAV-*Mettl5*-flag injection (bregma: 0.74 to −0.10 mm; interaural: 4.54 to 3.70 mm). Scale bar: 2 mm. (D) Immunofluorescent image of GFP$^+$ in transverse sections of the C5 spinal cord from mice 28 days after unilateral injury. (E) Quantification of GFP$^+$ corticospinal tract (CST) axons between groups (n = 6 each). (F) Immunofluorescence images of GFP$^+$ CST axons in the C6–7 spinal cord from wild type mice treated with AAV-DIO-mCherry or AAV-*Mettl5*-flag 28 days after unilateral injury. Scale bar: 500 μm (upper), 60 μm (lower). (G) Quantification of midline crossing GFP$^+$ CST axons (n = 6 each). Data are presented as means with standard deviation and were compared using the unpaired Student's *t*-test. ***$p < 0.001$, **$p < 0.01$, *$p < 0.05$. CST: corticospinal tract; TBI: traumatic brain injury; WT: wild type; AAV: adeno-associated virus; ns: not significant.

2.12. Immunofluorescence

Following fixation with 4 % PFA in PBS, the cells in the 24-well plates were washed three times with PBS and blocked with Quick-Block Blocking Buffer for 10 min. Then, the cells were incubated with primary antibodies targeting βIII-tubulin (mouse, 1:500, Proteintech, Cat# 66375-1-Ig) and flag overnight at 4 °C, followed by secondary antibodies including Alexa Fluor 488-conjugated goat anti-mouse IgG and Alexa Fluor 555-conjugated goat anti-rabbit IgG for 2 h at room temperature. Nuclei were stained with DAPI for 15 min. Images were captured using a fluorescence microscope and evaluated as previously described (Kauer et al., 2022). From five images from three different wells from three independent culture experiments, the length of the longest axon (from the soma to the tip of the axon) was measured using ImageJ software and the axonal branches were calculated. An independent investigator who was blinded to the experimental groups conducted the analyses.

2.13. Plasmid construction

The full-length open reading frame of the flag-tagged mouse *Mettl5* gene (NM_029280.4) was cloned into the pLVX vector to overexpress METTL5.

2.14. Statistical analysis

Statistical analyses were conducted using SPSS software version 20.0 (IBM Corp., USA). Data are presented as means with standard deviation. Groups were compared using the unpaired Student's *t*-test. $P < 0.05$ was considered significant.

3. Results

3.1. METTL5 promotes CST sprouting in mice after unilateral TBI

To evaluate whether overexpression of METTL5 in intact CSNs could drive intact CST sprouting, we injected either AAV-*Mettl5*-flag and AAV-GFP or AAV-DIO-mCherry (control) and AAV-GFP into the right M1 regions of WT mice 2 weeks before the unilateral TBI procedure (Fig. 1A). After injury, the mice exhibited characteristic neurological deficits, such as failing to fully extend the impaired forepaw and circling around the impaired side. These deficits persisted until the endpoint of the study. On day 28 after injury, the mice were sacrificed and processed for pathologic examination. On gross examination, the focal lesion was localized in the left M1 region (Fig. 1B) and immunofluorescence showed that almost all CSTs labeled by PKCγ in the C5 spinal cord were detected on the unparalyzed side (Fig. 1C). These results confirmed the successful establishment of a unilateral TBI mouse model.

On day 3 after injury, the mice in both groups exhibited a significant increase in missed step rate and asymmetry index, indicating neurological deficits. Subsequently, these behavioral parameters improved gradually over time. Notably, mice treated with AAV-*Mettl5*-flag exhibited significantly better recovery from day 7 to day 28 (Fig. 2A and B). The *Mettl5*-flag was localized at the injection site (Fig. 2C). Immunofluorescence showed a consistent number of GFP$^+$ CST axons in the C5 spinal cord regardless of control or treatment (Fig. 2D and E). However, the number of axons sprouting to the paralyzed side in the

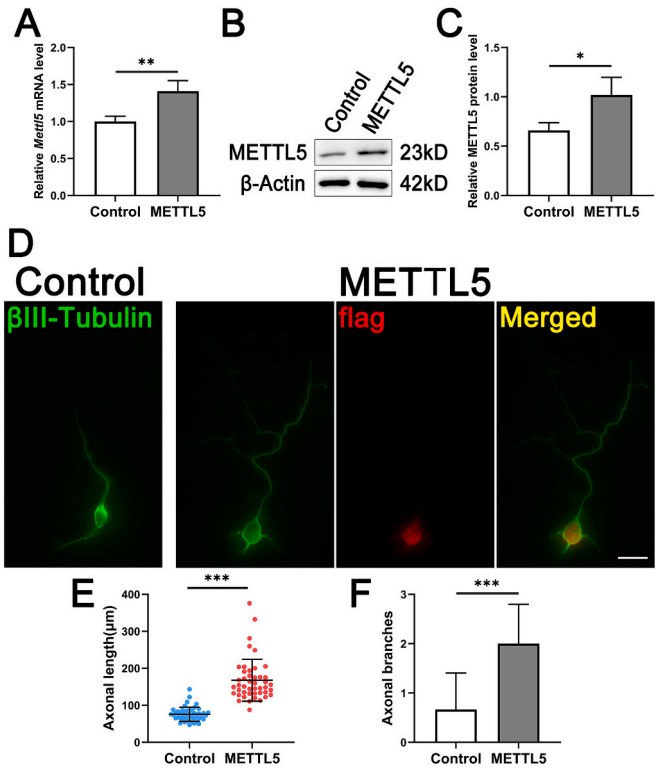

Fig. 3. METTL5 promotes axon outgrowth *in vitro*. (A) qRT-PCR analysis of *Mettl5*'s mRNA level in E17 wild type (WT) cortical neurons transfected with blank or *Mettl5*-flag plasmids after a 3-day cultivation period ($n = 3$ each). (B) Validation of METTL5 in E17 WT cortical neurons transfected with blank or *Mettl5* plasmids after a 3-day cultivation period using western blot assays. (C) Quantification of METTL5 levels related to (A) (n = 3 each). (D) Immunofluorescent image of the morphology of E17 WT cortical neurons transfected with blank or *Mettl5*-flag plasmids after a 3-day cultivation period. Scale bar = 40 μm. (E) Quantification of the axonal length in (D) ($n = 45$ each); (F) Quantification of the axonal branches in (D) (n = 45 each). Data are presented as means with standard deviation and were compared using the unpaired Student's t-test. ***p < 0.001, **p < 0.01, *p < 0.05. E17: embryos at 17 days; WT: wild type; ns: not significant.

C6–7 spinal cord was greater in the AAV-*Mettl5*-flag treatment group than the control group (Fig. 2F and G). These data suggest that METTL5 promotes both behavioral outcomes and CST sprouting after unilateral TBI.

3.2. *METTL5 promotes axon outgrowth in cortical neurons*

To evaluate whether METTL5 facilitates axon outgrowth *in vitro*, dissociated E17 cortical neurons were transfected with *Mettl5*-flag or blank plasmids. After a 3-day cultivation period, cortical neurons were harvested for qRT-PCR, western blotting, and immunofluorescence assays. Overexpression of METTL5 in cortical neurons was validated using both qRT-PCR (Fig. 3A) and western blot assays (Fig. 3B and C). Cortical neurons transfected with *Mettl5*-flag grew significantly longer neurites with more branches compared with control neurons (Fig. 3D to F). These data suggest that METTL5 can promote axon outgrowth in cortical neurons.

3.3. *METTL5 promotes expression of cofilin and its activity*

METTL5 is the methyltransferase responsible for 18S rRNA m^6A modification at site 1832. The SELECT assay results demonstrated that overexpression of METTL5 led to an increase in 18S rRNA m^6A modification at site 1832 in cortical neurons (Fig. 4A). Existing studies have shown that METTL5-mediated 18S rRNA m^6A modification promotes TE of specific mRNAs (Peng et al., 2022; Dai et al., 2023; Rong et al., 2020). To explore the key downstream factors for axon outgrowth regulated by METTL5, RNA-seq and RNC-seq were performed on the WT cortical neurons transfected with *Mettl5*-flag or blank plasmids after a 3-day cultivation period. RNA-seq data identified 274 genes with upregulated transcription levels and 323 genes with downregulated transcription levels (Fig. 4B). However, Gene Ontology analysis indicated that the genes with upregulated transcriptional levels were not significantly enriched in the processes related to axon outgrowth (Fig. 4C). In contrast, RNC-seq data revealed a more pronounced impact on the TEs of genes, with 3141 genes presenting upregulated TEs and 5036 genes showing downregulated TEs (Fig. 4D). Of note, Gene Ontology analysis indicated that the genes with upregulated TEs were significantly enriched in the processes related to axon outgrowth (Fig. 4E). Importantly, actin filament (F-actin) polymerization is the crucial process that facilitates axon outgrowth *via* remodeling of the actin cytoskeleton (Schneider et al., 2023). In addition, active cofilin (nonphosphorylated form) is the key regulator of F-actin polymerization (Namme et al., 2021). We found that the gene *Cfl1*, which encodes cofilin, was significantly upregulated in TE when METTL5 was overexpressed; however, its transcriptional level remained constant (RNA-seq: $p < 0.001$, fold change = 1.116; RNC-seq: TE ratio = 1.611), and thus we selected cofilin as a representative target of METTL5-mediated 18S rRNA m^6A modification. The qRT-PCR assay result showed that METTL5 overexpression had little effect on cofilin's mRNA level (Fig. 4F); however, a significant increase in its TE was confirmed by using RNC-mRNAs and their input samples (Fig. 4G). Further western blot assays revealed that METTL5 overexpression significantly increased protein levels of total cofilin (including both dephosphorylated and phosphorylated forms) and active cofilin (Fig. 4H and I). Although the protein level of inactive cofilin (phosphorylated form) exhibited a decreased trend, this did not reach statistical significance (Fig. 4H and I). A recent study has identified INPP5K as an important factor in activating cofilin (Kauer et al., 2022). In our investigation, we found that *Inpp5k* was significantly upregulated in TE upon METTL5 overexpression (TE ratio = 1.850), as was its protein product, INPP5K (Fig. 4J and K), which may be mechanisms that result in cofilin activation. Together, our data reveal that METTL5-mediated 18S rRNA m^6A modification enhances the expression level and activity of cofilin, potentially through the increased TE of cofilin's mRNA and cofilin activation *via* INPP5K. These may be the key downstream targets for METTL5's role in promoting axon outgrowth *in vitro* and CST sprouting *in vivo*.

4. Discussion

METTL5 is the only methyltransferase for 18S rRNA m^6A modification at site 1832; moreover, there is no evidence to suggest it exerts an effect on other coding or non-coding RNA (van Tran et al., 2019; Sepich-Poore et al., 2022). METTL5 exhibits *in vitro* activity towards full-length 18S rRNA and its activity increases 100-fold in the presence of TRMT112 (Oerum et al., 2021). METTL5-mediated 18S rRNA m^6A facilitates ribosome synthesis and mRNA translation (Sepich-Poore et al., 2022), while depletion of METTL5 markedly inhibits global mRNA translation (Peng et al., 2022; Dai et al., 2023). However, the detailed mechanism remains poorly understood. Previous studies have reported that rRNA modifications are commonly located in conserved functional sites, indicating that rRNA modifications are instrumental in ribosome maturation, thus regulating mRNA translation (Sloan et al., 2017; Polikanov et al., 2015).

Although many previous studies of METTL5 were conducted in the setting of oncology (Peng et al., 2022; Dai et al., 2023; Rong et al., 2020; Xia et al., 2023), its roles in neural development and function have been gaining interest. Mutations of *Mettl5* result in intellectual disability and microcephaly (Richard et al., 2019). *Mettl5* deficiency leads to disorientation during flying behavior in Drosophila (Leismann et al., 2020).

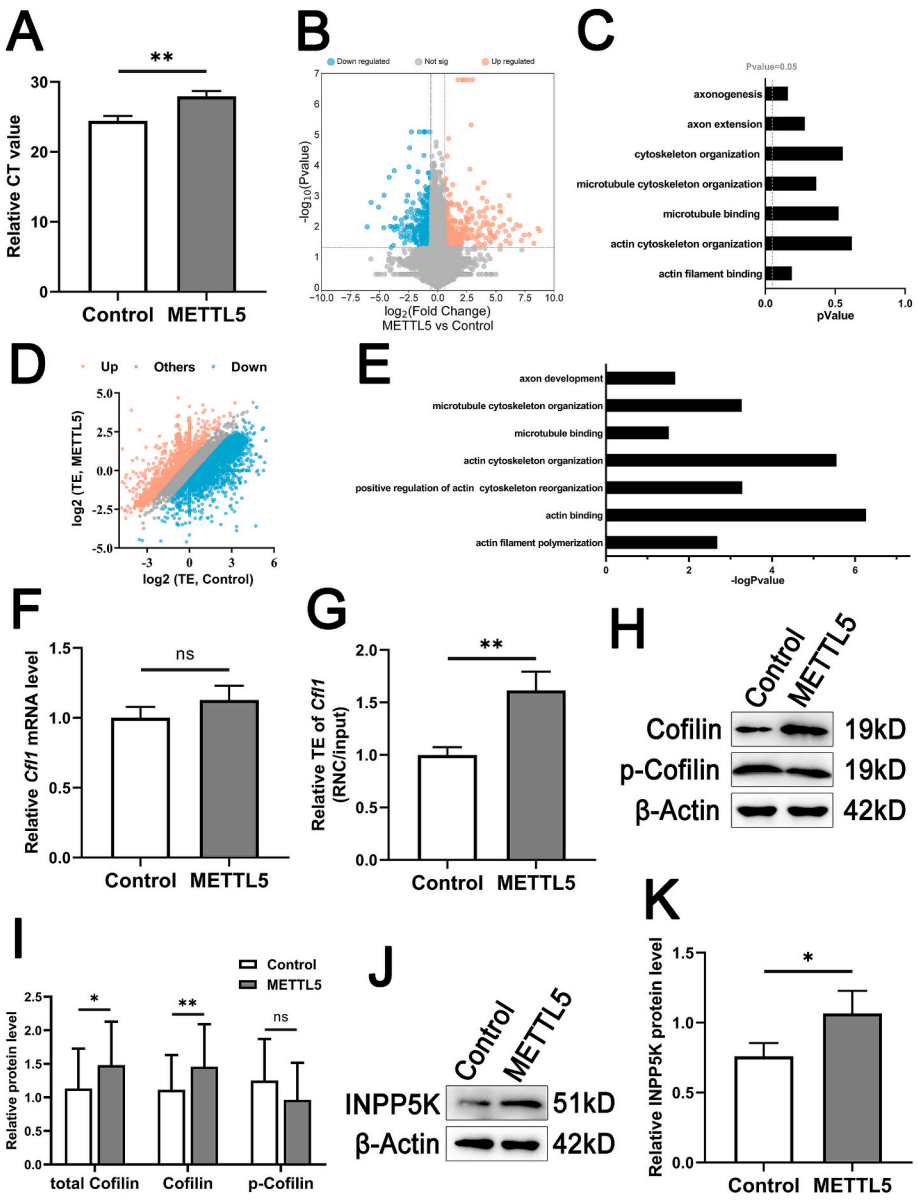

Fig. 4. METTL5 promotes the expression of cofilin and its activity. (A) Comparison of the levels of 18S rRNA m^6A modification at site 1832 in E17 cortical neurons transfected with blank or *Mettl5*-flag plasmids after a 3-day cultivation period using SELECT assay (n = 3 each). (B) Volcano Plot of RNA-Seq data from E17 wild type (WT) cortical neurons transfected with blank or *Mettl5*-flag plasmids after a 3-day cultivation period (n = 3 each). (C) Gene Ontology analysis of genes with upregulated transcriptional level upon METTL5 overexpression. (D) Scatterplot of RNC-seq from E17 WT cortical neurons transfected with blank or *Mettl5*-flag plasmids after a 3-day cultivation period ($n = 2$ each). (E) Gene Ontology analysis of genes with upregulated TE caused by METTL5 overexpression. (F and G) qRT-PCR analysis of *Cfl1*'s mRNA (F) and relative TE (G) in E17 WT cortical neurons transfected with blank or *Mettl5*-flag plasmids after a 3-day cultivation period (n = 3 each). (H) Validation of cofilin and phosphorylated cofilin in E17 WT cortical neurons transfected with blank or *Mettl5* plasmids after a 3-day cultivation period using western blot assays. (I) Quantification of total cofilin (including both dephosphorylated and phosphorylated forms), cofilin, and phosphorylated cofilin levels related to (H) (n = 3 each). (J) Validation of INPP5K in E17 cortical neurons transfected with blank or *Mettl5* plasmids after a 3-day cultivation period using western blot assays. (I) Quantification of INPP5K levels related to (J) (n = 3 each). Data are presented as means with standard deviation and were compared using the unpaired Student's t-test. ***p < 0.001, **p < 0.01, *p < 0.05. SELECT: single-base elongation and ligation-based PCR amplification; E17: embryos at 17 days; WT: wild type; TE: translation efficiency; ns: not significant.

Moreover, knockout of *Mettl5* leads to abnormal nervous system development in mouse embryonic stem cells and intellectual disability in mice (Wang et al., 2022). Our study elucidates the role of METTL5 in CST sprouting after unilateral TBI, adding a new dimension to the understanding of its function.

Intact CST sprouting is a key mechanism for the functional recovery of a paralyzed limb after brain injury. However, its underlying mechanisms remain elusive. Studies have suggested that several factors that promote axon regeneration also have a positive influence on axon sprouting, such as brain-derived neurotrophic factor (Ueno et al., 2012), inosine (Chen et al., 2002) and Nogo-A (Lindau et al., 2014). These findings suggest that the mechanisms underlying axon regeneration and sprouting exhibit a degree of similarity. Inherently, regeneration is the process for remodeling of the axonal cytoskeleton (consisting of neurofilaments, F-actin and microtubules) (Hur and Saijilafu, 2012), meaning that it may also have an impact on sprouting.

Cofilin, an essential protein for F-actin depolymerization, is highly concentrated in growth cones; it is activated *via* dephosphorylation and deactivated *via* phosphorylation (Schneider et al., 2023). Active cofilin promotes axon outgrowth (Frendo et al., 2019; Tedeschi et al., 2019;

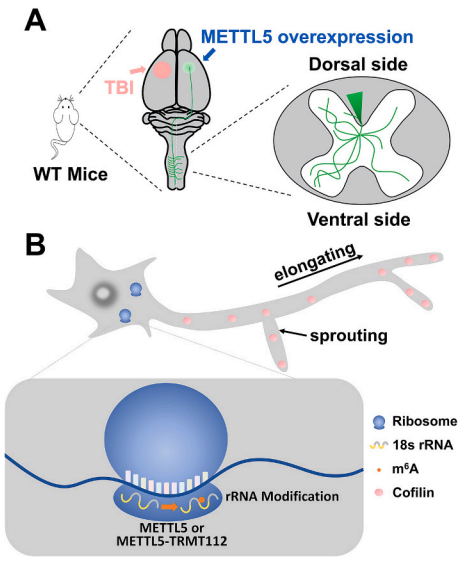

Fig. 5. Working model. (A) Overexpression of METTL5 in contralesional corticospinal neurons promotes corticospinal tract sprouting after unilateral TBI. (B) METTL5-mediated 18S rRNA m6A modification promotes the expression of cofilin and its activity, potentially through increased translation efficiency of cofilin's mRNA and activation of cofilin *via* the upregulated TE of INPP5K. TBI: traumatic brain injury.

Sudarsanam et al., 2020). Active cofilin disassembles F-actin and the subsequent actin turnover allows the radial orientation of F-actin, facilitating protrusion and bundling of microtubules into the growth cone (Flynn et al., 2012). Microtubule protrusion into the growth cone periphery accelerates axon outgrowth (Dupraz et al., 2019). In contrast, absence of cofilin results in disorganization of F-actin, which leads to looped and disorganized trajectories (Kauer et al., 2022). In our study, METTL5-mediated 18S rRNA m^6A modification promoted the TE of cofilin's mRNA, resulting in an increase in its expression. Meanwhile, the upregulated TE of INPP5K caused by METTL5 overexpression appears to underly activation of cofilin. Based on these data, we propose that cofilin is a key downstream target for METTL5's role in promoting CST sprouting after unilateral TBI. However, our study faced a limitation in that we were unable to perform rescue experiments for further verification because of a lack of *Mettl5* knockout/knockin mice.

5. Conclusion

This study unveiled METTL5's promoting effect on intact CST sprouting after unilateral TBI. Mechanically, METTL5-mediated 18S rRNA m^6A modification enhanced the TE of cofilin's mRNA, leading to an increase in its expression. Additionally, the upregulation of TE in INPP5K's mRNA led to activation of cofilin. Active cofilin appears to promote axon outgrowth by stimulating actin polymerization and facilitating protrusion and bundling of microtubules. These findings may offer valuable insights for developing novel strategies to facilitate CST sprouting after unilateral brain injury (Fig. 5).

Funding

This study was supported by the National Key Research and Development Program of China (2022YFC2602800), the National Natural Science Foundation of China (82201523), the Guangdong Basic and Applied Basic Research Foundation (2024A1515013183), and the Guangzhou Municipal Science and Technology Project (202201010775, 2023A04J2186).

CRediT authorship contribution statement

Zhenpeng Li: Writing – review & editing, Writing – original draft, Visualization, Validation, Software, Methodology, Investigation, Formal analysis, Data curation. **An Jiang:** Methodology, Investigation. **Jintao Fang:** Writing – review & editing, Methodology, Investigation, Funding acquisition, Formal analysis, Data curation. **Yifei Jiang:** Methodology, Investigation. **Wenting He:** Investigation, Funding acquisition. **Liwei Yan:** Investigation. **Shuai Qiu:** Investigation, Funding acquisition. **Bengang Qin:** Writing – review & editing, Supervision, Resources. **Qingtang Zhu:** Writing – review & editing, Supervision, Resources. **Honggang Wang:** Writing – review & editing, Visualization, Supervision, Resources, Project administration, Funding acquisition, Conceptualization.

Declaration of competing interest

The authors declare that they have no known competing financial interest or personal relationships that could have appeared to influence the work reported in this paper.

Acknowledgements

This study received assistance from the Center for Translational Medicine, Precision Medicine Institute, The First Affiliated Hospital, Sun Yat-sen University. We also thank Topbiotech Biotechnology Co., Ltd. (Guangzhou, China) for providing support for the animal experimental platform, and Liwen Bianji (Edanz) (https://www.liwenbianji.cn) for editing the English text of a draft of this manuscript.

Data availability

The accession number of raw sequencing data deposited in the NCBI Sequence Read Archive (SRA) is: PRJNA1161207. The remaining data used in this study are available from the corresponding author upon reasonable request.

References

Bakalkin, G., Nosova, O., Sarkisyan, D., Hallberg, M., Zhang, M., Schouenborg, J., et al., 2021. Unilateral traumatic brain injury of the left and right hemisphere produces the left hindlimb response in rats. Exp. Brain Res. 239, 2221–2232.
Benowitz, L.I., Carmichael, S.T., 2010. Promoting axonal rewiring to improve outcome after stroke. Neurobiol. Dis. 37, 259–266.
Biernaskie, J., Szymanska, A., Windle, V., Corbett, D., 2005. Bi-hemispheric contribution to functional motor recovery of the affected forelimb following focal ischemic brain injury in rats. Eur. J. Neurosci. 21, 989–999.
Boato, F., Guan, X., Zhu, Y., Ryu, Y., Voutounou, M., Rynne, C., et al., 2023. Activation of MAP2K signaling by genetic engineering or HF-rTMS promotes corticospinal axon sprouting and functional regeneration. Sci. Transl. Med. 15, eabq6885.
Chen, P., Goldberg, D.E., Kolb, B., Lanser, M., Benowitz, L.I., 2002. Inosine induces axonal rewiring and improves behavioral outcome after stroke. Proc. Natl. Acad. Sci. USA 99, 9031–9036.
Chen, P., Zhang, T., Yuan, Z., Shen, B., Chen, L., 2019. Expression of the RNA methyltransferase Nsun5 is essential for developing cerebral cortex. Mol. Brain 12, 74.
Dai, Z., Zhu, W., Hou, Y., Zhang, X., Ren, X., Lei, K., et al., 2023. METTL5-mediated 18S rRNA m(6)a modification promotes oncogenic mRNA translation and intrahepatic cholangiocarcinoma progression. Mol. Ther. 31, 3225–3242.
Duechler, M., Leszczyńska, G., Sochacka, E., Nawrot, B., 2016. Nucleoside modifications in the regulation of gene expression: focus on tRNA. Cell. Mol. Life Sci. 73, 3075–3095.
Dupraz, S., Hilton, B.J., Husch, A., Santos, T.E., Coles, C.H., Stern, S., et al., 2019. RhoA controls axon extension independent of specification in the developing brain. Curr. Biol. 29, 3874–3886.
Fink, K.L., López-Giráldez, F., Kim, I.J., Strittmatter, S.M., Cafferty, W.B.J., 2017. Identification of intrinsic axon growth modulators for intact CNS neurons after injury. Cell Rep. 18, 2687–2701.
Flynn, K.C., Hellal, F., Neukirchen, D., Jacob, S., Tahirovic, S., Dupraz, S., et al., 2012. ADF/cofilin-mediated actin retrograde flow directs neurite formation in the developing brain. Neuron 76, 1091–1107.
Frendo, M.E., da Silva, A., Phan, K.D., Riche, S., Butler, S.J., 2019. The Cofilin/Limk1 pathway controls the growth rate of both developing and regenerating motor axons. J. Neurosci. 39, 9316–9327.

Gao, Z., Pang, Z., Lei, G., Chen, Y., Cai, Z., Zhu, S., et al., 2022. Crossing nerve transfer drives sensory input-dependent plasticity for motor recovery after brain injury. Sci. Adv. 8, eabn5899.
Hur, E.M., Saijilafu, Zhou F.Q., 2012. Growing the growth cone: remodeling the cytoskeleton to promote axon regeneration. Trends Neurosci. 35, 164–174.
Jin, D., Liu, Y., Sun, F., Wang, X., Liu, X., He, Z., 2015. Restoration of skilled locomotion by sprouting corticospinal axons induced by co-deletion of PTEN and SOCS3. Nat. Commun. 6, 8074.
Kauer, S.D., Fink, K.L., Li, E.H.F., Evans, B.P., Golan, N., Cafferty, W.B.J., 2022. Inositol Polyphosphate-5-phosphatase K (Inpp5k) enhances sprouting of corticospinal tract axons after CNS trauma. J. Neurosci. 42, 2190–2204.
Leismann, J., Spagnuolo, M., Pradhan, M., Wacheul, L., Vu, M.A., Musheev, M., et al., 2020. The 18S ribosomal RNA m(6) a methyltransferase Mettl5 is required for normal walking behavior in Drosophila. EMBO Rep. 21, e49443.
Liepert, J., Bauder, H., Wolfgang, H.R., Miltner, W.H., Taub, E., Weiller, C., 2000. Treatment-induced cortical reorganization after stroke in humans. Stroke 31, 1210–1216.
Lindau, N.T., Bänninger, B.J., Gullo, M., Good, N.A., Bachmann, L.C., Starkey, M.L., et al., 2014. Rewiring of the corticospinal tract in the adult rat after unilateral stroke and anti-Nogo-a therapy. Brain 137, 739–756.
Liu, Z., Xin, H., Chopp, M., 2021. Axonal remodeling of the corticospinal tract during neurological recovery after stroke. Neural Regen. Res. 16, 939–943.
Murphy, T.H., Corbett, D., 2009. Plasticity during stroke recovery: from synapse to behaviour. Nat. Rev. Neurosci. 10, 861–872.
Namme, J.N., Bepari, A.K., Takebayashi, H., 2021. Cofilin signaling in the CNS physiology and neurodegeneration. Int. J. Mol. Sci. 22, 10727.
Noller, H.F., 1991. Ribosomal RNA and translation. Annu. Rev. Biochem. 60, 191–227.
Oerum, S., Meynier, V., Catala, M., Tisné, C., 2021. A comprehensive review of m6A/m6Am RNA methyltransferase structures. Nucleic Acids Res. 49, 7239–7255.
Pandolfi, P.P., 2004. Aberrant mRNA translation in cancer pathogenesis: an old concept revisited comes finally of age. Oncogene 23, 3134–3137.
Peng, H., Chen, B., Wei, W., Guo, S., Han, H., Yang, C., et al., 2022. N(6)-methyladenosine (m(6)a) in 18S rRNA promotes fatty acid metabolism and oncogenic transformation. Nat. Metab. 4, 1041–1054.
Polikanov, Y.S., Melnikov, S.V., Söll, D., Steitz, T.A., 2015. Structural insights into the role of rRNA modifications in protein synthesis and ribosome assembly. Nat. Struct. Mol. Biol. 22, 342–344.
Richard, E.M., Polla, D.L., Assir, M.Z., Contreras, M., Shahzad, M., Khan, A.A., et al., 2019. Bi-allelic variants in METTL5 cause autosomal-recessive intellectual disability and microcephaly. Am. J. Hum. Genet. 105, 869–878.
Romaus-Sanjurjo, D., Saikia, J.M., Kim, H.J., Tsai, K.M., Le, G.Q., Zheng, B., 2022. Overexpressing eukaryotic elongation factor 1 alpha (eEF1A) proteins to promote corticospinal axon repair after injury. Cell Death Dis. 8, 390.
Rong, B., Zhang, Q., Wan, J., Xing, S., Dai, R., Li, Y., et al., 2020. Ribosome 18S m(6)a methyltransferase METTL5 promotes translation initiation and breast Cancer cell growth. Cell Rep. 33, 108544.
Schneider, F., Metz, I., Rust, M.B., 2023. Regulation of actin filament assembly and disassembly in growth cone motility and axon guidance. Brain Res. Bull. 192, 21–35.
Schosserer, M., Minois, N., Angerer, T.B., Amring, M., Dellago, H., Harreither, E., et al., 2015. Methylation of ribosomal RNA by NSUN5 is a conserved mechanism modulating organismal lifespan. Nat. Commun. 6, 6158.
Sepich-Poore, C., Zheng, Z., Schmitt, E., Wen, K., Zhang, Z.S., Cui, X.L., et al., 2022. The METTL5-TRMT112 N(6)-methyladenosine methyltransferase complex regulates mRNA translation via 18S rRNA methylation. J. Biol. Chem. 298, 101590.
Sloan, K.E., Warda, A.S., Sharma, S., Entian, K.D., Lafontaine, D.L.J., Bohnsack, M.T., 2017. Tuning the ribosome: the influence of rRNA modification on eukaryotic ribosome biogenesis and function. RNA Biol. 14, 1138–1152.
Starkey, M.L., Bleul, C., Zörner, B., Lindau, N.T., Mueggler, T., Rudin, M., et al., 2012. Back seat driving: hindlimb corticospinal neurons assume forelimb control following ischaemic stroke. Brain 135, 3265–3281.
Sudarsanam, S., Yaniv, S., Meltzer, H., Schuldiner, O., 2020. Cofilin regulates axon growth and branching of Drosophila γ-neurons. J. Cell Sci. 133, jcs232595.
Tedeschi, A., Dupraz, S., Curcio, M., Laskowski, C.J., Schaffran, B., Flynn, K.C., et al., 2019. ADF/Cofilin-mediated actin turnover promotes axon regeneration in the adult CNS. Neuron 103, 1073–1085.
Ueno, M., Hayano, Y., Nakagawa, H., Yamashita, T., 2012. Intraspinal rewiring of the corticospinal tract requires target-derived brain-derived neurotrophic factor and compensates lost function after brain injury. Brain 135, 1253–1267.
van Tran, N., Ernst, F.G.M., Hawley, B.R., Zorbas, C., Ulryck, N., Hackert, P., et al., 2019. The human 18S rRNA m6A methyltransferase METTL5 is stabilized by TRMT112. Nucleic Acids Res. 47, 7719–7733.
Wang, T., Cui, Y., Jin, J., Guo, J., Wang, G., Yin, X., et al., 2013. Translating mRNAs strongly correlate to proteins in a multivariate manner and their translation ratios are phenotype specific. Nucleic Acids Res. 41 (9), 4743–4754.
Wang, L., Liang, Y., Lin, R., Xiong, Q., Yu, P., Ma, J., et al., 2022. Mettl5 mediated 18S rRNA N6-methyladenosine (m(6)a) modification controls stem cell fate determination and neural function. Genes Dis. 9, 268–274.
Wang, D., Zheng, T., Zhou, S., Liu, M., Liu, Y., Gu, X., et al., 2023. Promoting axon regeneration by inhibiting RNA N6-methyladenosine demethylase ALKBH5. eLife 12, e85309.
Wu, Y., Wu, H., Zeng, J., Pluimer, B., Dong, S., Xie, X., et al., 2021. Mild traumatic brain injury induces microvascular injury and accelerates Alzheimer-like pathogenesis in mice. Acta Neuropathol Commun. 9, 74.
Xia, X., Wang, Y., Zheng, J.C., 2023. Internal m7G methylation: a novel epitranscriptomic contributor in brain development and diseases. Mol Ther Nucleic Acids. 31, 295–308.
Xia, P., Zhang, H., Lu, H., Xu, K., Jiang, X., Jiang, Y., et al., 2023. METTL5 stabilizes c-Myc by facilitating USP5 translation to reprogram glucose metabolism and promote hepatocellular carcinoma progression. Cancer Commun (Lond). 43, 338–364.
Yang, Y., Chen, X., Yang, C., Liu, M., Huang, Q., Yang, L., et al., 2024. Chemogenetic stimulation of intact corticospinal tract during rehabilitative training promotes circuit rewiring and functional recovery after stroke. Exp. Neurol. 371, 114603.
Yuan, Z., Chen, P., Zhang, T., Shen, B., Chen, L., 2019. Agenesis and Hypomyelination of Corpus callosum in mice lacking Nsun5, an RNA methyltransferase. Cells 8, 552.
Zhao, B.S., Roundtree, I.A., He, C., 2017. Post-transcriptional gene regulation by mRNA modifications. Nat. Rev. Mol. Cell Biol. 18, 31–42.
Zheng, M.X., Hua, X.Y., Feng, J.T., Li, T., Lu, Y.C., Shen, Y.D., et al., 2018. Trial of contralateral seventh cervical nerve transfer for spastic arm paralysis. N. Engl. J. Med. 378, 22–34.
Zhu, B., Gu, G., Ren, J., Song, X., Li, J., Wang, C., et al., 2023. Schwann cell-derived exosomes and methylprednisolone composite patch for spinal cord injury repair. ACS Nano 17, 22928–22943.